Adaptive Airfoils for Drag Reduction at Transonic Speeds

David W. Zingg,* Laslo Diosady† and Laura Billing,‡
Institute for Aerospace Studies, University of Toronto
4925 Dufferin St., Toronto, Ontario M3H 5T6, Canada

Adaptive airfoils and wings can provide superior performance at the expense of increased cost and complexity. In this paper, an aerodynamic optimization algorithm is used to assess an adaptive airfoil concept for drag reduction at transonic speeds. The objective is to quantify both the improvements in drag that can be achieved and the magnitude of the shape changes needed. In an initial study, a baseline airfoil is designed to produce low drag at a fixed lift coefficient over a range of Mach numbers. This airfoil is compared with a sequence of nine airfoils, each designed to be optimal at a single operating point in the Mach number range. Shape changes of less than 2% chord lead to drag reductions of 4-6% over a range of Mach numbers from 0.68 to 0.76. If the shape changes are restricted to the upper surface only, then changes of less than 1% chord lead to drag reduction of 3-5%. In a second study, a baseline airfoil is designed based on a multi-point optimization over eighteen operating points, including dive and low-speed off-design requirements. Adaptive airfoils are designed through single-point optimization for the operating points corresponding to cruise conditions, producing drag reductions ranging from 9.7 to 16.7% with shape changes on the order of a few percent chord.

I. Introduction

Projected increases in air travel combined with rising fuel costs and environmental concerns have led to renewed interest in drag reduction. One of the difficulties in designing an efficient wing is the requirement that the wing be able to operate efficiently in several different areas of the flight envelope. While it is accepted that flaps and possibly slats be deployed for take-off, climb, and landing, a single wing shape is used for most other conditions. For example, a wing must operate over a range of flight Mach numbers and a range of lift coefficients. In addition, satisfactory performance is required under dive and high-lift conditions. This leads to a complex multi-point multi-objective optimization problem, and the resulting wing's performance at a given condition is compromised by the need for good performance under other conditions.

One possible solution to this difficulty is a morphing wing in which the wing shape is altered depending on the flight condition. This is an expensive and complex proposition and hence can only be considered if the resulting performance benefits are substantial, and the required shape changes are relatively small. Stanewsky[1] provides a thorough review of adaptive wing and flow control technology, including practical aspects. Trenker[2] studied deformable airfoils for unsteady flows suitable for helicopter rotors. Distributed piezoelectric actuators are examined by Anusonti-Inthra et al.[3] as a means of deforming airfoils, again with application to helicopter rotors. Recently, Patzold et al.[4] studied shock control bumps using numerical optimization. Namgoong et al.[5] also applied a numerical optimization technique to the design of a morphing airfoil in an interesting study in which morphing energy requirements were included in the objective function to be minimized.

In this paper we apply a modern aerodynamic shape optimization algorithm based on the Reynolds-averaged Navier-Stokes equations[6,7] to determine both a fixed baseline airfoil which provides good performance over a range of operating conditions as well as a family of adaptive airfoils suitable for use at specific

*Professor, Senior Canada Research Chair in Computational Aerodynamics, Senior AIAA Member.
†Undergraduate Student (currently a graduate student at the Massachusetts Institute of Technology)
‡Graduate Student

operating conditions. The objective is to quantify both the benefits of the adaptive airfoil and the magnitude of the shape changes needed. This information is needed to assess the viability of the concept. First we consider operation at fixed lift over a range of Mach numbers. Next a broader range of operating conditions is examined, including variable Mach number, variable lift coefficient, and some off-design requirements.

II. Newton-Krylov Algorithm For Aerodynamic Shape Optimization

The Newton-Krylov approach of Nemec and Zingg[6,7] is briefly described. For a complete description, see Nemec.[8] The geometry is parameterized through B-splines. The B-spline control points and the angle of attack are the design variables. The compressible Navier-Stokes equations are solved with a Newton-Krylov method in which the linear system arising at each Newton iteration is solved using the generalized minimal residual method (GMRES) preconditioned with an incomplete lower-upper (ILU) factorization with limited fill. The Spalart-Allmaras turbulence model is used to compute the eddy viscosity. The gradient is calculated using the discrete adjoint method; solution of the adjoint equation is accomplished through the same preconditioned Krylov method. Geometric constraints are added to the objective function as penalty terms. A new set of design variables is computed using a quasi-Newton optimizer in which an estimate of the inverse Hessian based on the BFGS (Broyden-Fanno-Goldfarb-Shannon) rank-two update formula is used to compute a search direction.[9] If the initial step does not produce sufficient progress toward the minimum, the step size is determined using a line search, which terminates when the strong Wolfe conditions are satisfied.[9] Each time a new shape is calculated, the initial grid is perturbed using a simple algebraic technique.

The accuracy of our flow solver has been studied extensively, and the present meshes can be expected to produce lift coefficients accurate to within 1% and drag coefficients to within 5% for attached and mildly separated flows.[10] More importantly in the present context, differences in drag are predicted even more accurately, i.e. if the drag coefficient computed for two airfoils on comparable meshes differs by a certain percentage, then the drag coefficient computed for the same airfoils on finer but again comparable meshes will typically differ by the same percentage to within less than one percent.

III. Lift-Constrained Drag Minimization: Multi-Point Optimization

We seek to optimize an airfoil for minimum drag at a fixed lift coefficient of 0.725 over a range of Mach numbers from 0.68 to 0.76. The Reynolds number is 2.7 million. Although it is possible to design an airfoil that produces no shock waves at a specific Mach number in the prescribed range, it is not possible to obtain shock-free flows for the entire range with a single airfoil.

The objective function for lift-constrained drag minimization is given by:

$$J_{\mathrm{d}} = \begin{cases} \omega_{\mathrm{L}} \left(1 - \frac{C_{\mathrm{L}}}{C_{\mathrm{L}}^*}\right)^2 + \omega_{\mathrm{D}} \left(1 - \frac{C_{\mathrm{D}}}{C_{\mathrm{D}}^*}\right)^2 & \text{if } C_{\mathrm{D}} > C_{\mathrm{D}}^* \\ \omega_{\mathrm{L}} \left(1 - \frac{C_{\mathrm{L}}}{C_{\mathrm{L}}^*}\right)^2 & \text{otherwise} \end{cases} \tag{1}$$

where C_{L}^* is a target lift coefficient, C_{D}^* is a target drag coefficient, and ω_{L} and ω_{D} are weights. Choosing a target lift coefficient that is attainable and a target drag coefficient that is unattainable with suitable weights leads to lift-constrained drag minimization with the lift constraint treated as a penalty term.

The target lift coefficient, C_{L}^*, is chosen to be 0.733, slightly higher than the desired lift value of 0.725. Fully turbulent flow is assumed, i.e. transition is assumed to occur at the leading edge. The initial geometry is the RAE 2822 airfoil. Forty B-spline control points are used to parameterize the geometry. Two control points are frozen at the leading edge and two at the trailing edge. Hence there are 37 design variables, including the angle of attack. The following thickness constraints are imposed in order to prevent crossover: $t/c \geq 0.01$ at $x/c = 0.02$, $t/c \geq 0.001$ at $x/c = 0.99$, $t/c \geq 0.00001$ at $x/c = 0.998$. In addition, the cross-sectional area is constrained to be no less than the area of the initial RAE 2822 airfoil section in order to provide suitable internal volume for fuel storage as well as adequate structural properties.

In order to determine the baseline airfoil, we use the following composite objective function:

$$J = J_{M=0.68} + J_{M=0.71} + J_{M=0.73} + J_{M=0.75} + J_{M=0.76} \tag{2}$$

where J_M is the objective function given by Eq. 1 evaluated at the Mach number indicated. The five different operating points are equally weighted. As long as the drag is well behaved between operating points, this approximates an unweighted integral over the operating range.

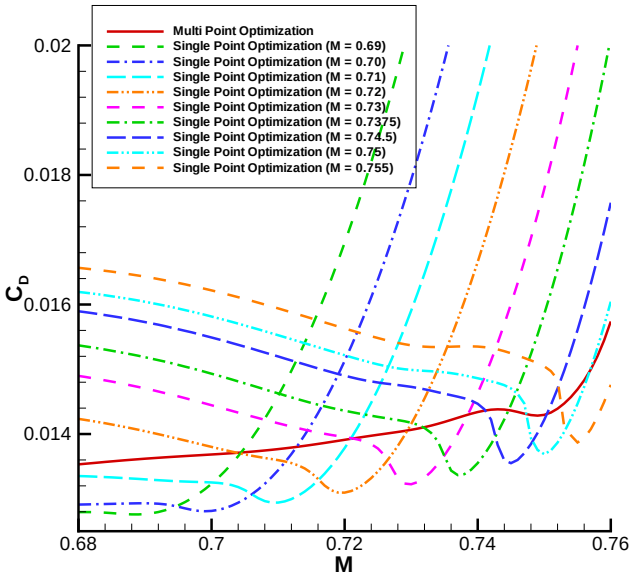

Figure 1. C_d **vs. Mach number at** $C_l = 0.725$**: multi-point optimization and adaptive airfoils.**

A 289×65 mesh with an off-wall spacing of 2×10^{-6} chords was generated about the initial geometry using an elliptic mesh generator. After completing an optimization, a new mesh is generated about the modified airfoil, and the optimization is repeated. This reduces numerical errors that can result from reduced mesh quality associated with the algebraic mesh modifications. After the second optimization, a final mesh is generated and used to compute the drag coefficient on the optimized shape at a fixed lift coefficient of 0.725 for the entire Mach number range.

The resulting drag coefficient vs. Mach number curve at $C_l = 0.725$ is labelled "Multi Point Optimization" in Fig. 1. The drag coefficient increases with Mach number as a result of the equal weighting used. This weighting is somewhat arbitrary, and different weightings can be used. For example, Zingg and Elias[11] present an automated approach for optimizing an airfoil that produces a constant drag over the specified Mach number range. However, the present weighting provides an appropriate baseline for assessment of the adaptive airfoil concept. The airfoil is displayed in Fig. 2 with an expanded view in Fig. 3. The surface pressure coefficient distributions are plotted in Fig. 4 for several different Mach numbers. A weak shock wave exists on the upper surface at each Mach number.

IV. Adaptive Airfoils

The adaptive airfoil is designed by optimizing the shape at nine different Mach numbers: 0.69, 0.70, 0.71, 0.72, 0.73, 0.7375, 0.745, 0.75, and 0.755. The objective function in Eq. 1 is used, and the procedure followed is the same as that described above except that single-point optimization is performed. The baseline airfoil previously designed through multi-point optimization is used as the initial airfoil. Weights are adjusted to ensure that the area of each individual airfoil lies within 0.002% of the area of the baseline airfoil.

The resulting variation of the drag coefficient with Mach number at $C_l = 0.725$ is shown for each of the nine airfoils in Fig. 1. As one would expect of single-point optimization, each individual airfoil has a low drag coefficient over a narrow range of Mach numbers, roughly 6% lower than the drag coefficient of the baseline airfoil at the same Mach number, and a much higher drag coefficient over the remainder of the Mach number range. The airfoils are displayed in Figs. 2 and 3. Maximum movement of the upper surface is roughly 1.8% chord; maximum lower surface movement is roughly 1.2% chord. The corresponding pressure distributions are shown in Fig. 5. All are shock-free. Pitching moment coefficients are shown in Fig. 6. With one minor

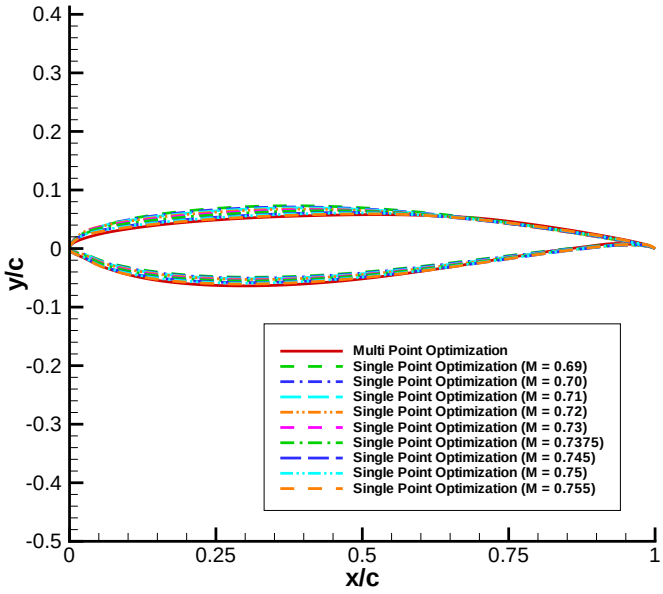

Figure 2. Airfoil sections: multi-point optimization and adaptive airfoils.

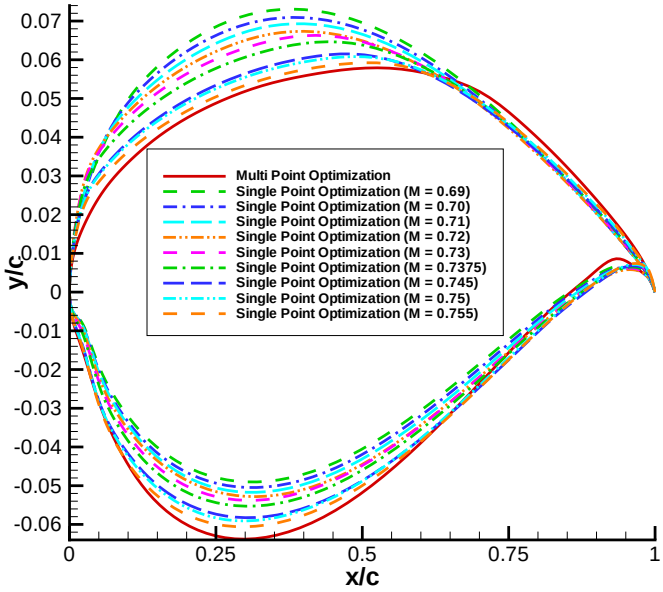

Figure 3. Expanded view of airfoil sections: multi-point optimization and adaptive airfoils.

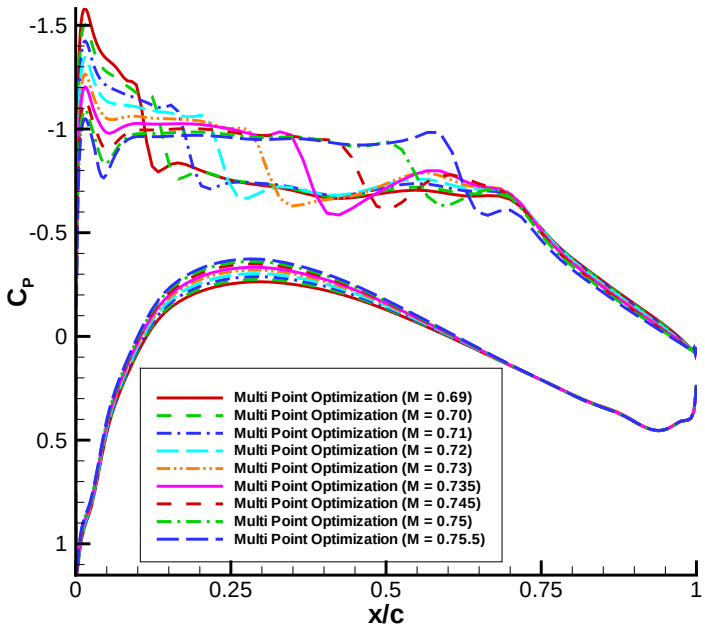

Figure 4. Pressure distributions: multi-point optimization.

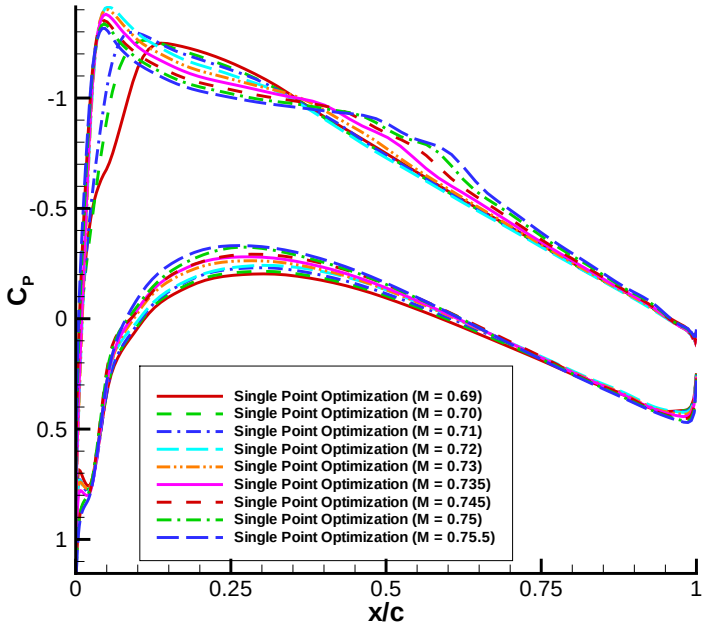

Figure 5. Pressure distributions: adaptive airfoils.

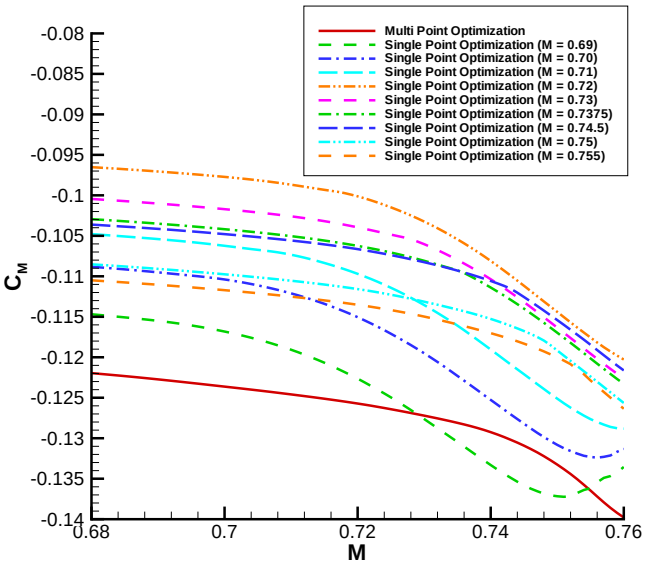

Figure 6. Pitching moment coefficient vs. Mach number: baseline airfoil and adaptive airfoils.

exception[a] the single-point optimized airfoils have smaller moment coefficients than the baseline airfoil.

Note that the present adaptive concept can be utilized in two different ways. When operating at a given Mach number, the shape can be altered to match the airfoil optimized at the Mach number closest to the given Mach number. Alternatively, one can determine a continuous variation of shape throughout the Mach number range.

V. Adaptive Airfoils: Upper Surface Variation Only

The above optimization exercise was repeated permitting only variation in the upper surface shape with the lower surface fixed to the baseline airfoil geometry designed through multi-point optimization. Specifically, the 15 B-spline control points defining the upper surface back to 90% chord were allowed to vary, giving 16 design variables including the angle of incidence. Care was again taken to ensure that the adaptive airfoils have areas within 0.002% of the area of the baseline airfoil. The motivation for freezing the lower surface is to simplify the mechanism for surface movement, thereby reducing cost and complexity.

The resulting drag coefficient variation with Mach number is plotted in Fig. 7. The drag reduction is somewhat smaller than when the entire airfoil can adapt, varying from 4% to 5.5% at the specified Mach numbers. Figs. 8 and 9 show the resulting airfoils. The movement of the upper surface is somewhat smaller, with a maximum of roughly 0.6%. The pressure distributions are all shock-free, as displayed in Fig. 10. Fig. 11 shows that the pitching moments are significantly smaller than those of the baseline airfoil.

VI. An Eighteen-Point Optimization

Next we consider a model eighteen-point optimization problem for a hypothetical airplane with the operating conditions given in Table 1. The first four operating points (A-D) correspond to cruise conditions at different altitudes with different aircraft weights. The objective for these four points is to minimize the drag coefficient with the specified lift coefficient. The next four operating points (E-H) correspond to long-range cruise, again with varying altitudes and weights. The objective is to minimize the product of the Mach number and the lift-to-drag ratio, but, since the Mach number and lift coefficient are specified, this

[a]which is not in a Mach number range where the given airfoil is optimized

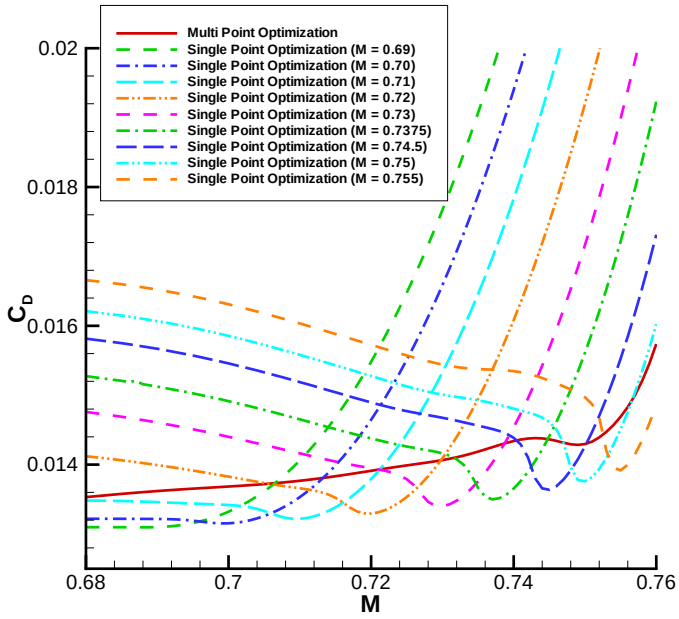

Figure 7. C_d **vs. Mach number at** $C_l = 0.725$**: multi-point optimization and adaptive airfoils with upper surface variation only.**

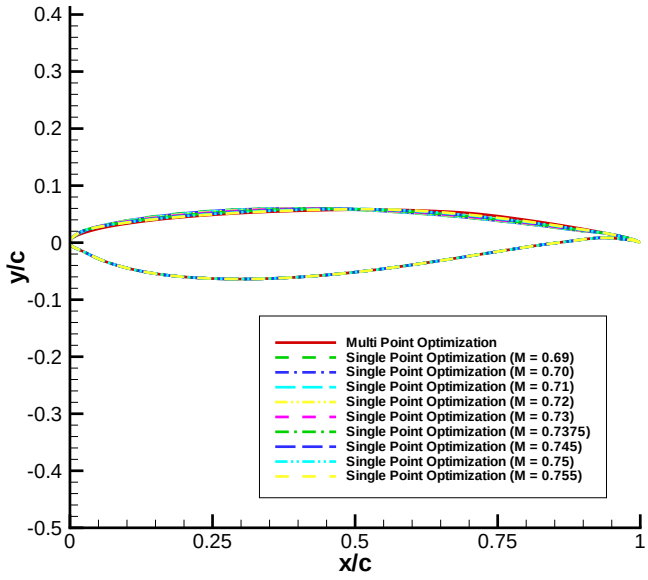

Figure 8. Airfoil sections: multi-point optimization and adaptive airfoils with upper surface variation only.

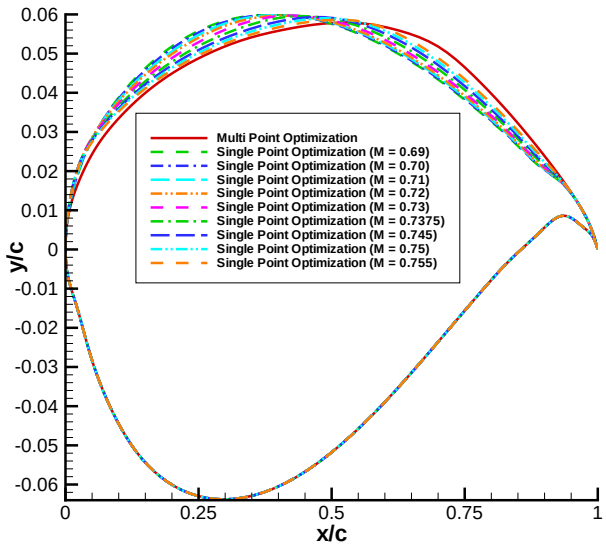

Figure 9. Expanded view of airfoil sections: multi-point optimization and adaptive airfoils with upper surface variation only.

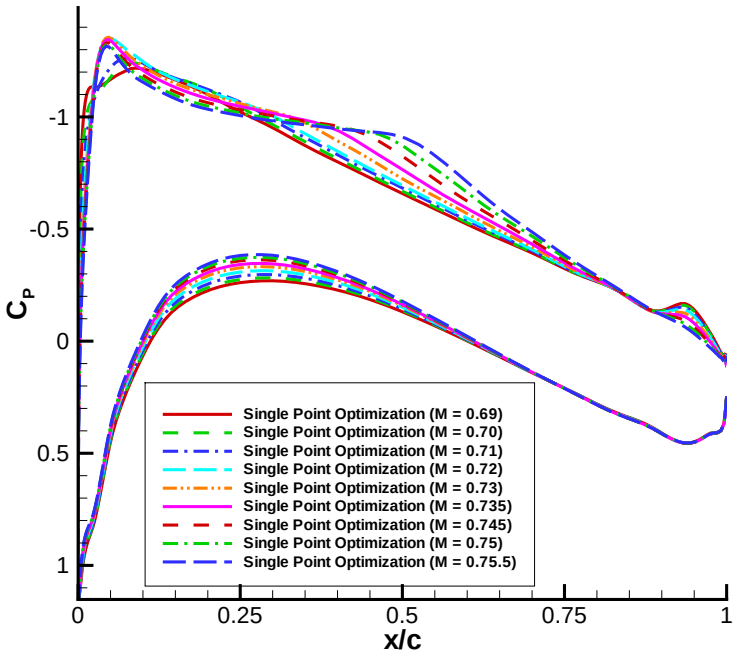

Figure 10. Pressure distributions: adaptive airfoils with upper surface variation only.

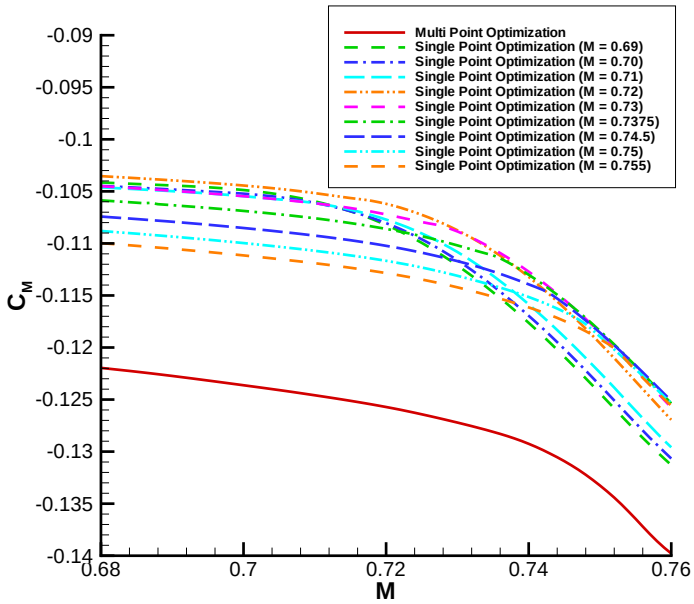

Figure 11. Pitching moment coefficient vs. Mach number: baseline airfoil and adaptive airfoils with upper surface variation only.

again requires that the drag coefficient be minimized. Note that the Mach numbers are based on a sweep angle of 35 degrees. The next eight operating points (I-P) correspond to dive conditions. The objective is to keep shock strengths modest, such that the upstream Mach number at all shocks is less than 1.35. The final two operating points correspond to low-speed operation. The objective is to ensure that the maximum lift coefficient under these conditions is at least 1.6. The last ten operating conditions are off-design and can be treated as constraints. In our formulation, constraints are added to the objective function as quadratic penalty terms, so some effort is required to find appropriate weights for these terms.

There is, of course, no unique solution to such a multi-point problem, since one can attach different weights to the various operating points. Furthermore, computing a solution to such a problem is a challenging task, and we defer a detailed discussion to a future paper. Here we concentrate on a particular solution obtained by manipulating the weights such that good performance is achieved for operating points A through H while meeting the requirements of points I through R. Drag minimization is used to reduce shock strengths.

The geometry is parameterized using 15 B-spline control points with the NACA 0015 as the initial geometry. Three control points are frozen at the leading edge and two at the trailing edge. Hence there are ten design variables, five on each surface. A floating thickness constraint of 14.2% chord is imposed to ensure a thickness of at least 14% chord. In addition, a thickness of 1% chord is imposed at 95% chord and 0.2% at 99% chord in order to prevent crossover. The meshes used have a C topology with 289 nodes in the streamwise direction and 65 in the normal direction. Fully turbulent flow is again assumed.

Table 2 summarizes the performance of the resulting airfoil, which is depicted in Figs. 12 and 13. For some of the off-design operating conditions, the performance exceeds the requirement. This indicates either that the weight on this point is too high or that the point is not critical, i.e. satisfactory performance is achieved even if the point is given zero weight. In the former case, a reduction in the weight could lead to an improvement at the on-design operating points (A-H). However, such improvement is likely to be small, since the most difficult off-design condition (operating point O) is the critical one, and it is just barely satisfied. Overall, the airfoil designed using the eighteen-point optimization provides excellent performance over the entire range of operating conditions. Pressure distributions for operating points A-H are shown in Figs. 14 and 15. It is interesting to note that the solutions are shock-free at all eight operating points.

Table 1. Operating conditions for eighteen-point optimization.

Operating Point	Reynolds Number	Mach Number	Lift Coefficient
A	27.32×10^6	0.72	0.17
B	27.32×10^6	0.72	0.28
C	18.57×10^6	0.72	0.27
D	18.57×10^6	0.72	0.45
E	24.22×10^6	0.64	0.21
F	24.22×10^6	0.64	0.36
G	16.46×10^6	0.64	0.34
H	16.46×10^6	0.64	0.57
I	28.88×10^6	0.76	0.28
J	28.88×10^6	0.76	0.15
K	28.88×10^6	0.76	0.46
L	28.88×10^6	0.76	0.25
M	19.62×10^6	0.76	0.45
N	19.62×10^6	0.76	0.24
O	19.62×10^6	0.76	0.74
P	19.62×10^6	0.76	0.40
Q	11.8×10^6	0.16	–
R	15.0×10^6	0.20	–

Table 2. Performance of airfoil designed through eighteen-point optimization. The maximum Mach number column gives the maximum local Mach number upstream of a shock wave.

Operating Point	C_l	C_d	Maximum Mach Number	$C_{l\max}$
A	0.17	0.0125	–	–
B	0.28	0.0126	–	–
C	0.27	0.0128	–	–
D	0.45	0.0134	–	–
E	0.21	0.0122	–	–
F	0.36	0.0125	–	–
G	0.34	0.0126	–	–
H	0.57	0.0136	–	–
I	0.28	0.0139	1.19	–
J	0.15	0.0143	1.26	–
K	0.46	0.0171	1.28	–
L	0.25	0.0138	1.17	–
M	0.45	0.0170	1.27	–
N	0.24	0.0139	1.17	–
O	0.74	0.0562	1.34	–
P	0.40	0.0158	1.25	–
Q	–	–	–	1.77
R	–	–	–	1.78

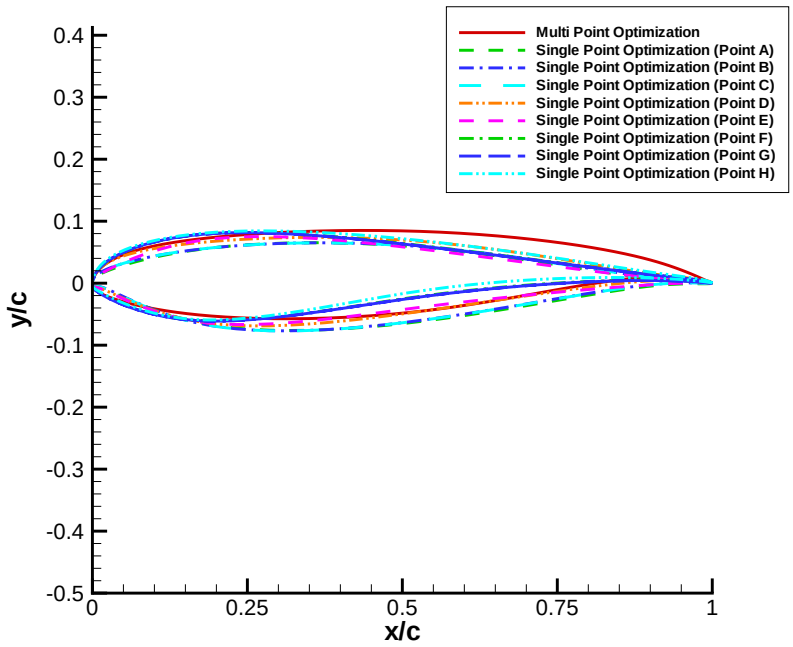

Figure 12. Airfoil sections: eighteen-point optimization and adaptive airfoils.

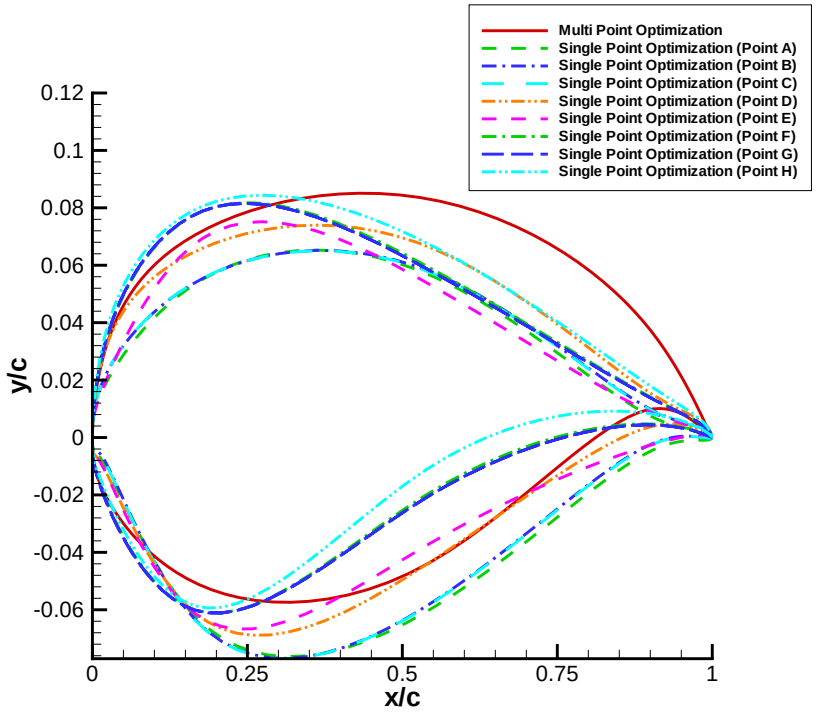

Figure 13. Expanded view of airfoil sections: eighteen-point optimization and adaptive airfoils.

Table 3. Comparison of drag coefficients of the single-point designs with those of the baseline multi-point design.

Operating Point	C_d (multi-point)	C_d (single-point)	% Reduction
A	0.0125	0.01038	16.7
B	0.0126	0.01077	14.6
C	0.0128	0.01088	14.8
D	0.0134	0.01187	11.7
E	0.0122	0.01093	10.1
F	0.0125	0.01100	11.8
G	0.0126	0.01104	12.2
H	0.0136	0.01228	9.7

VII. Single-Point Optimization

Next we consider single-point optimization at the cruise operating conditions (A-H) in Table 1. Design variables, thickness constraints, and meshes are the same as used for the eighteen-point optimization. Table 3 gives the performance of the resulting airfoils, which is substantially improved over the baseline airfoil designed using the multi-point optimization. The associated airfoil shapes and pressure distributions are displayed in Figs. 12, 13, 14, and 15. The drag coefficient at the cruise operating points (A-H) is reduced between 9.7 and 16.7%. This is a significant reduction in drag that is difficult to achieve by other means. In contrast to the previous example, where the drag reduction is primarily the result of shock elimination, the drag is strictly the result of viscous effects, and the drag reduction is achieved by reducing both pressure and friction drag. The shape changes are larger than those in the previous example. Although shape variation of this magnitude may not be practical, this study provides an upper bound on the benefits of this concept.

For some operating points, significant drag reductions can be achieved with much smaller shape changes. This is illustrated in Fig. 16, which shows the progress of the single-point optimization for operating point D, using the multi-point design as the initial shape. A reduction in drag of 8% can be obtained with a fairly small shape change; the movement of the lower surface is almost negligible.

VIII. Discussion and Conclusions

In our first example, we have demonstrated that with relatively small shape changes, drag reductions of 4-6% can be achieved over a range of Mach numbers from 0.68 to 0.76 relative to a baseline airfoil designed using multi-point optimization. Similarly, adaptive airfoils with shape changes on the upper surface only can achieve drag reductions of 4 to 5.5% over the same Mach number range. This shows that the basic concept is a promising means of addressing the pressing need for drag reduction at transonic speeds motivated by environmental concerns and rising fuel costs.

A practical airfoil must operate efficiently over not only a range of Mach numbers but also a range of lift coefficients. Furthermore, there are off-design requirements, such as low-speed high-lift and dive conditions. Consequently, the overall performance is compromised by many competing objectives, and therefore the benefits of adaptive airfoils can be significantly greater than the above assessment indicates. In our second example, we have presented a baseline airfoil designed to perform efficiently under a practical set of operating conditions and a comparison of its performance with adaptive airfoils designed using single-point optimization. In this case, the drag reduction achieved is larger, ranging from 9.7 to 16.7%. However, the required shape changes are also larger. Future work should concentrate on incorporating the shape changes into the objective function to minimize the complexity of the deformation mechanism and the energy requirements associated with the deformations.[5]

These results quantify the drag reduction possible using the adaptive airfoil concept, which is significant. This must be weighed against the energy consumed in adapting the wing, the increased cost and complexity, and the implications for safety. As the actuator technology needed to deform the wing improves, the price of fuel increases, and the need to reduce harmful emissions becomes more critical, the adaptive wing concept will become increasingly viable.

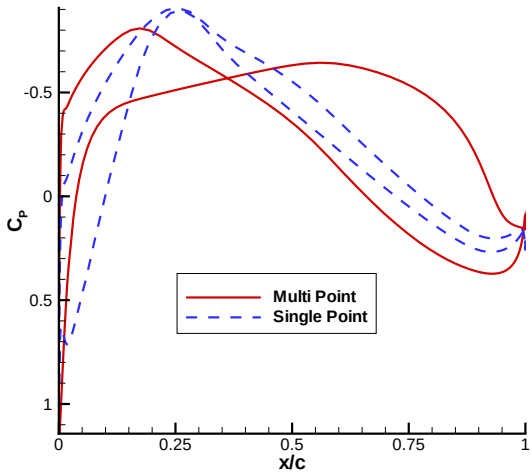

(a) Point A

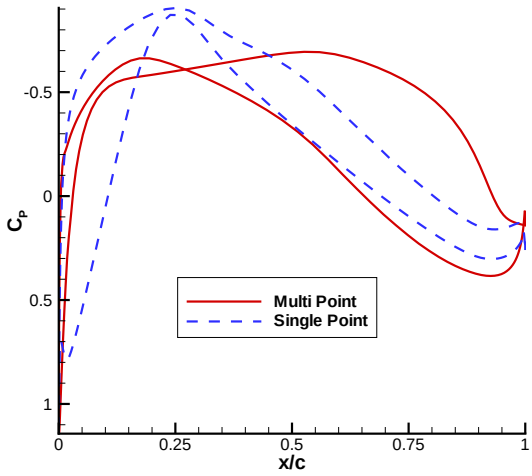

(b) Point B

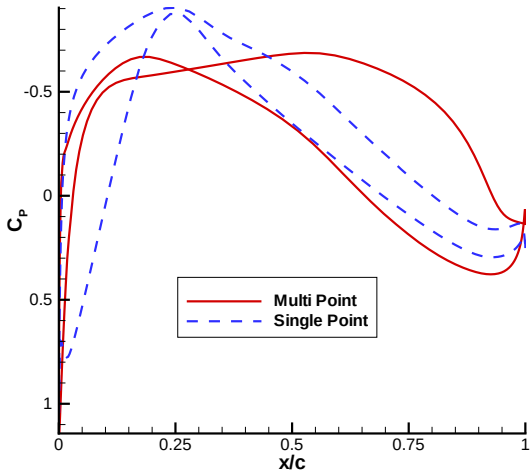

(c) Point C

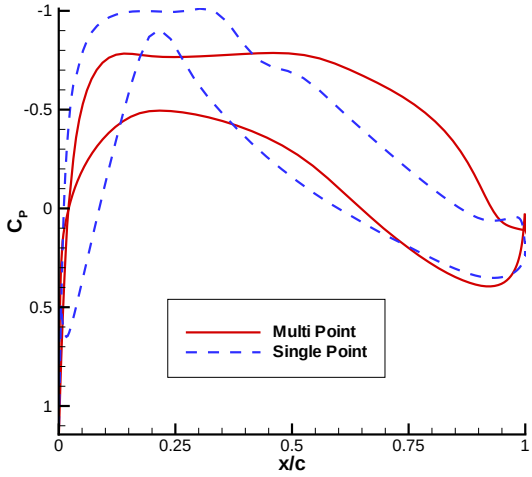

(d) Point D

Figure 14. Comparison of pressure distributions for single-point and multi-point optimized airfoils, operating points A–D.

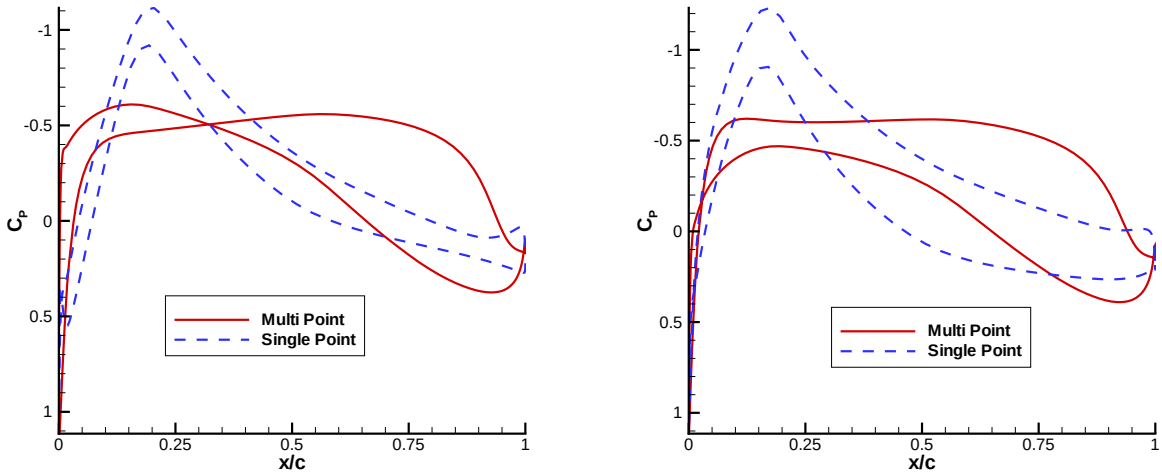

(a) Point E

(b) Point F

(c) Point G

(d) Point H

Figure 15. Comparison of pressure distributions for single-point and multi-point optimized airfoils, operating points E–H.

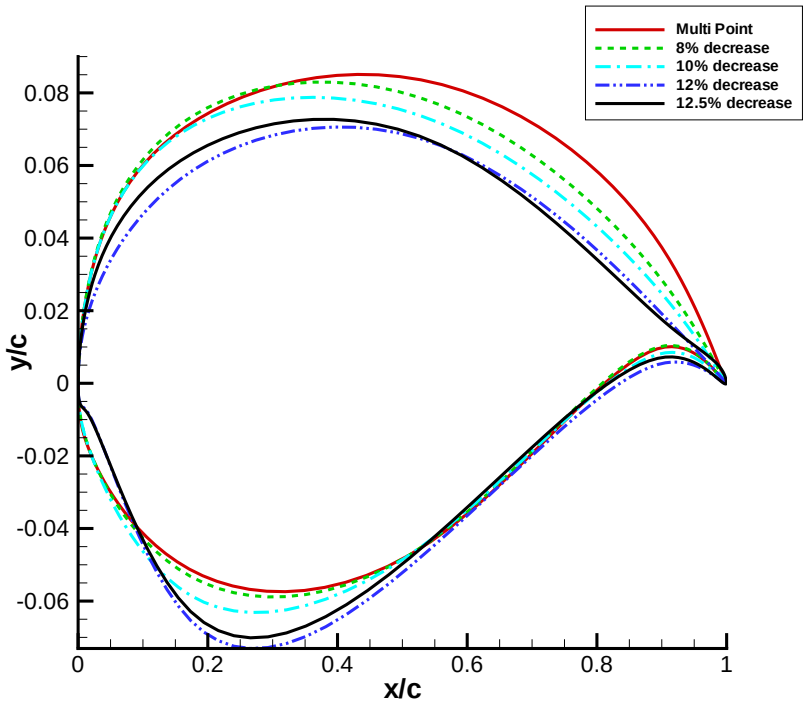

Figure 16. Expanded view of airfoil sections for operating point D showing the progress of the single-point optimization. The legend gives the drag reduction compared to the multi-point design.

Acknowledgments

The funding of the first author by the Natural Sciences and Engineering Research Council of Canada and the Canada Research Chairs program is gratefully acknowledged.

References

[1]Stanewsky, E., "Adaptive Wing and Flow Control Technology," *Progress in Aerospace Sciences*, Vol. 37, 2001, pp. 583-667.

[2]Trenker, M., "Design Concepts for Adaptive Airfoils with Dynamic Transonic Flow Control," *Journal of Aircraft*, Vol. 40, No. 4, 2003, pp. 734-740.

[3]Anusonti-Inthra, P., Sarjeant, R., Frecker, M., and Gandhi, F., "Design of a Conformable Rotor Airfoil Using Distributed Piezoelectric Actuators," *AIAA J.*, Vol. 43, No. 8, 2005, pp. 1684-1695.

[4]Patzold, M., Lutz, T., Kramer, E., and Wagner, S., "Numerical Optimization of Finite Shock Control Bumps," AIAA Paper 2006-1054, Jan. 2006.

[5]Namgoong, H., Crossley, W.A., and Lyrintzis, A.S., "Aerodynamic Optimization of a Morphing Airfoil Using Energy as an Objective," AIAA Paper 2006-1324, Jan. 2006.

[6]Nemec, M., and Zingg, D.W., "Newton-Krylov Algorithm for Aerodynamic Design Using the Navier-Stokes Equations," *AIAA J.*, Vol. 40, No. 6, 2002, pp. 1146-1154.

[7]Nemec, M., Zingg, D.W., and Pulliam, T.H., "Multipoint and Multi-Objective Aerodynamic Shape Optimization," *AIAA J.*, Vol. 42, No. 6, 2004, pp. 1057-1065.

[8]Nemec, M., "Optimal Shape Design of Aerodynamic Configurations: A Newton-Krylov Approach," Ph.D. Thesis, University of Toronto Institute for Aerospace Studies, 2002.

[9]Nocedal, J. and Wright, S.J., *Numerical Optimization*, Springer-Verlag, New York, 1999.

[10]Zingg, D.W., "Grid Studies for Thin-Layer-Navier-Stokes Computations of Airfoil Flowfields," Tech. Note, *AIAA J.*, Vol. 30, No. 10, pp. 2561-2564, 1992.

[11]Zingg, D.W., and Elias, S., "On Aerodynamic Optimization Under a Range of Operating Conditions," AIAA Paper 2006-1053, Jan. 2006.